Obstacle-Aided Navigation of a Soft Growing Robot

Joseph D. Greer[1], Laura H. Blumenschein[1], Allison M. Okamura[1], and Elliot W. Hawkes[2]

***Abstract*— For many types of robots, avoiding obstacles is necessary to prevent damage to the robot and environment. As a result, obstacle avoidance has historically been an important problem in robot path planning and control. Soft robots represent a paradigm shift with respect to obstacle avoidance because their low mass and compliant bodies can make collisions with obstacles inherently safe. Here we consider the benefits of intentional obstacle collisions for soft robot navigation. We develop and experimentally verify a model of robot-obstacle interaction for a tip-extending soft robot. Building on the obstacle interaction model, we develop an algorithm to determine the path of a growing robot that takes into account obstacle collisions. We find that obstacle collisions can be beneficial for open-loop navigation of growing robots because the obstacles passively steer the robot, both reducing the uncertainty of the location of the robot and directing the robot to targets that do not lie on a straight path from the starting point. Our work shows that for a robot with predictable and safe interactions with obstacles, target locations in a cluttered, mapped environment can be reached reliably by simply setting the initial trajectory. This has implications for the control and design of robots with minimal active steering.**

I. Introduction

Motivated by goals of safety and efficiency, there is a large body of research on obstacle avoidance using robotic motion planning and control [1], [2]. This work includes avoidance of static and moving obstacles for nonholonomic robots and robot swarms [3], [4], [5]. However, for soft robots, obstacle avoidance is often less relevant than it is for rigid-bodied robots because the low inertia and compliant bodies of soft robots make obstacle collisions less dangerous for both the robot and object [6]. In applications such as search and rescue and inspection, which involve navigation of cluttered or constrained environments, obstacle interaction may be unavoidable and even advantageous. In these scenarios, a system that allows for and utilizes robot-obstacle interaction is desirable.

Estimating, compensating for, and understanding the impact of contact with obstacles is an important task for serial manipulators, which has been addressed by a large body of work [7], [8], [9]. In the area of soft robotics, Coevoet et al. [10] predict deformations of soft robots caused by environmental contact, and the model-less control strategy for tendon-based manipulators of Yip and Camarillo [11] performs online estimation of a tip Jacobian. For mobile robots, models have been developed to predict the effects of interactions with obstacles while moving through unknown environments [12], [13].

This work was supported in part by the National Science Foundation (grant no. 1637446) and Department of Defense (grant no. FA2386-17-1-4658)

[1]Mechanical Engineering, Stanford University
[2]Mechanical Engineering, University of California, Santa Barbara
email: jdgreer@stanford.edu

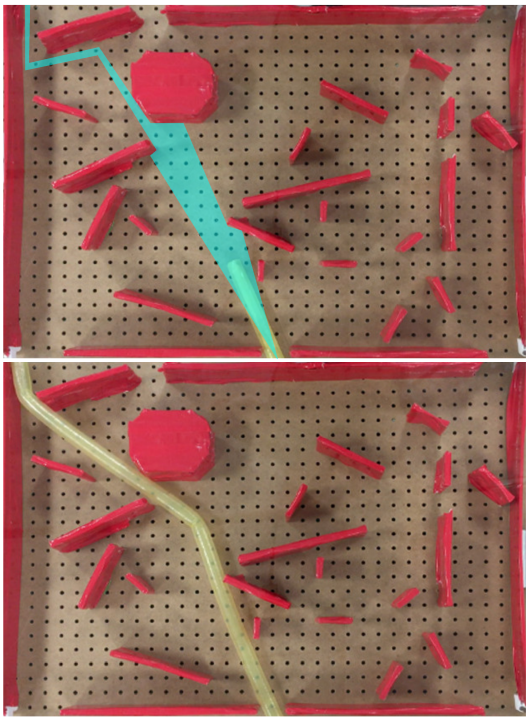

Fig. 1. We present a heuristic model that enables computation of paths that involve contact between a soft growing robot and the environment. We find that obstacles can be beneficial for navigation of a robot because they serve to passively guide the robot and reduce uncertainty in its motion. This is illustrated by the region of robot trajectories (top, cyan) being narrowed to a single path. The extended robot is shown (bottom).

Other research examines using obstacles to the benefit of the robot. For example, hyper-redundant snake robots could actively use obstacles in their environment to propel the snake robot forward and thereby aid locomotion [14], [15], [16] . Another class of robot that uses environmental constraints to benefit mobility is pipe robots. It is only at pipe junctions that the robots have to make navigation decisions, otherwise they are directed along a path set by the shape of their environment [17].

Our work falls into this second category of research that uses obstacles to benefit the robot. In particular, we investigate how obstacle collisions affect navigation of a tip-extending, or "growing," soft robot (Fig. 1). These robots are inspired by organisms in nature that grow from the tip, such as vines and developing neurons, and have rich interactions with obstacles in their environment. In previous work, we developed an approach for realizing growth in a robot using pneumatically driven tip eversion [18] (Fig. 2(a)). Using this

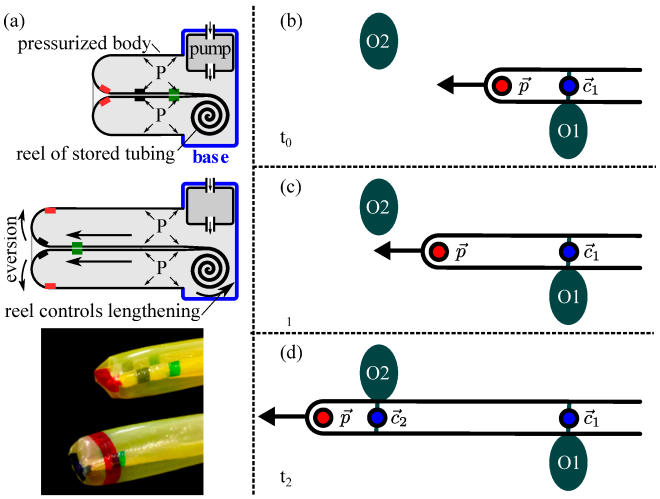

Fig. 2. (a) A schematic shows the concept of a tip-extending, or "growing" robot, based on an inverted pressurized tube that everts at the tip. Image of growing body shown at bottom. Adapted from [18]. (b-d) Model states of the lumped parameter model consist of the tip point, $\vec{p}$, and contact points $\vec{c}_1, \ldots, \vec{c}_n$. Obstacles in this figure are labeled O1 and O2. Pictures show the robot at three progressive time steps. From (b) to (c), point $\vec{p}$ moves with the robot's tip, and $\vec{c}_1$ is constant. From (c) to (d), $\vec{p}$ moves with the robot's tip and $\vec{c}_2$ is added to indicate a more distal point of the robot's backbone, which is in contact with obstacle O2.

method, we demonstrated extension of the growing robot by about 250 times the robot body's original length. Advantages of movement by growth include a stationary power source, no sliding friction and the ability to penetrate tight and cluttered spaces. These advantages are due to the fact that a growing robot's body does not need to slide with respect to its environment to move.

In this paper, we formalize interactions between these tip-extending robots and planar obstacles (i.e. obstacles that are extruded along the third dimension). First, Section II gives a differential kinematic interaction model that describes infinitesimal motions of the robot when in contact with an obstacle. Second, Section III describes an algorithm to compute the predicted path of a robot that is interacting with obstacles. Then, Section IV presents experiments that verify the interaction model with various obstacles and show that the path computation model can predict trajectories of the soft growing robot in a cluttered environment. Finally, in Section V, we discuss the implications of our results, limitations of the model, and future work.

II. Obstacle Interaction Model

In this section, we develop a simple heuristic model that describes the differential kinematics of a soft growing robot that is in contact with its environment. A soft growing robot consists of a pneumatic backbone that can extend in length and a turning mechanism that allows the growing robot to be steered from a straight-line trajectory to a destination. Several mechanisms have been proposed to steer a growing robot, including asymmetric lengthening of the robot's backbone at discrete intervals along its length [18] as well as constant curvature bending of a growing robot's backbone induced by pneumatic artificial muscles that are attached along the pneumatic backbone's length [19], [20], [21]. Because we are interested in understanding obstacle interactions for growing robots in general, we do not consider active steering in this analysis. However, this work could be incorporated into a motion model of an actively steered robot with little modification.

The growing robot in this paper belongs to the class of snake-like robots with flexible bodies known as continuum robots. Precise models of the kinematics and dynamics of continuum robots are developed using continuum mechanics theory such as Cosserat rod theory [22] and the finite-element method [10]. These methods are computationally expensive and rely on material parameters that may be difficult to estimate and change with time. A less exact, but simpler approximate modeling method that has been successfully used for certain continuum robots are lumped parameter models. These models characterize a continuum robot by specially chosen points along the robot's backbone. Examples of lumped parameter models of continuum robots include the unicycle model developed by Park et al. [23] as well as the bicycle model developed by Webster et al. [24], both for steerable needles. We also use a lumped-parameter model in this paper.

A. Model States

Our lumped-parameter model of the growing robot characterizes its state by specifically chosen points along the robot's backbone labeled $\vec{p}$ and $\vec{c_1}, \ldots, \vec{c_n}$ (Fig. 2). Point $\vec{p}$, called the tip point, is defined as the position of the robot's tip and $\vec{c}_1, \ldots, \vec{c}_n$, called contact points, are defined as the points of the robot's backbone that are in contact with obstacles and are distinct from $\vec{p}$. If there is more than one contact point per obstacle, the model stores the most distal point of contact between each obstacle and the robot backbone. Note that n varies with the number of contact points, and that a new contact point is not generated for an obstacle while the tip of the robot is in contact with it. The contact points are ordered most proximal ($\vec{c}_1$) to most distal ($\vec{c}_n$). The line segment from $\vec{c}_n$ to $\vec{p}$ represents the most distal segment of the growing robot.

B. Differential Kinematics of the Model

1) Free Growth: Free growth occurs when the tip of the growing robot is not in contact with an obstacle. Because active turning is not considered, the tip of the robot will extend in the direction of the most distal segment of the backbone, which is parallel to $\vec{p} - \vec{c}_n$. We write the free growth differential kinematics simply as

$$\dot{\vec{p}} = u \frac{1}{||\vec{p} - \vec{c}_n||} (\vec{p} - \vec{c}_n), \tag{1}$$

where u is the growth speed (rate of change of robot length), which we assume is controlled. Note that $\vec{c}_1, \ldots, \vec{c}_n$ are always updated to reflect the current contact points between the growing robot and environment.

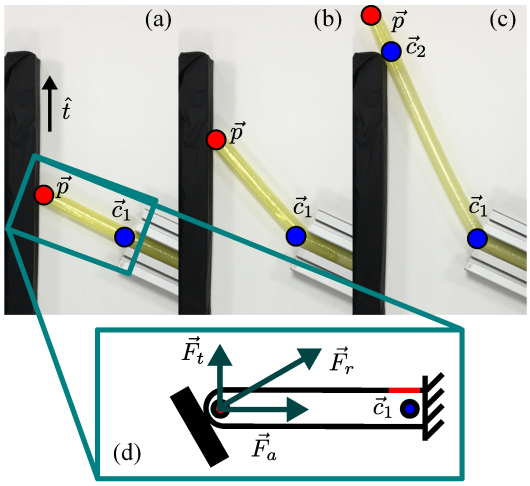

Fig. 3. Interaction of the robot and a obstacle. Robot shown at three successive time-steps (a-c). In (a), the robot comes into contact with the obstacle, after which the robot tip starts moving along direction $\hat{t}$, parallel to the obstacle surface, pivoting about point $\vec{c}_1$ (shown in b). In (c), the robot has grown past the obstacle, and resumes free-growth kinematics with an updated pivot point, $\vec{c}_2$. (d) Obstacle will exert a reaction force, $\vec{F}_r$, that has a transverse component. This will cause buckling about point $\vec{c}_n$ at the red highlighted surface.

2) Obstacle Contact: In this section, we describe a model for movement of the growing robot when its tip is in contact with an obstacle. We assume that the growing robot will approach the obstacle in free growth as depicted in Fig. 3. When the growing robot comes into contact with the obstacle, it will switch from free growing kinematics to obstacle contact kinematics.

We treat the growing robot as an inflatable beam constrained at point $\vec{c}_n$ with a reaction force, $\vec{F}_r$, applied by the obstacle to the robot's tip. $\vec{F}_r$ acts normal to the obstacle surface (and $\hat{t}$), and is shown in Fig. 3(d). The reaction force has components that are both transverse and parallel to the robot's backbone ($\vec{F}_t, \vec{F}_a$ respectively), both of which could cause the inflated beam to buckle. $\vec{F}_t$ will cause a transverse beam buckling at the base [25], while $\vec{F}_a$ will cause an axial buckling half way along the beam [26]. The magnitude of the critical buckling force for each of these two modes depends on many parameters, such as the pressure, wall thickness and material, length, and diameter, but for pressures less than 15 kPa, wall material of low density polyethylene with thickness on the order of 0.05 mm, free length less than a meter, and diameter on the order of 20 mm, transverse buckling at the base will occur in any case when the angle between the obstacle and the robot is greater than several degrees [27].

Therefore, once a bending moment that is larger than the compressed air in the tube can resist is applied, the robot's backbone will buckle at the point $\vec{c}_n$. The net effect is that the tip of the robot will move tangent to the obstacle's surface (parallel to $\hat{t}$), pivoting about point $\vec{c}_n$. Internal pressure in the robot will ensure that its tip will remain in contact with the obstacle until it grows past the obstacle's edge. When this happens, the robot will switch back to free growth kinematics and a new contact point will be added to reflect the new point of contact between the robot and the obstacle it grew along.

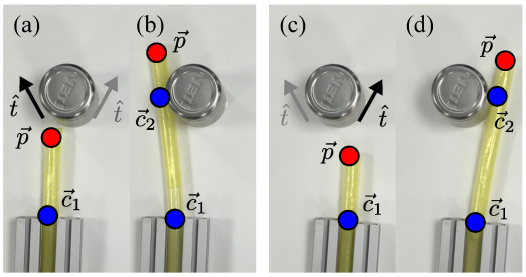

Fig. 4. Growing robot obstacle interaction kinematics with a round obstacle. The reaction forces of the obstacle will direct the robot to the left (a-b) or right side (c-d) of the obstacle depending on where the robot initially makes contact with the obstacle since the obstacle's contour tangent directions (denoted by $\hat{t}$) spatially vary over the obstacle boundary.

Figs. 3 and 4 show the robot tip interacting with a wall and cylinder, respectively. The robot's tip flows around the obstacles, and once past, its trajectory is dictated by the pivot point, $\vec{c}_n$. Obstacle interaction differential kinematics are expressed mathematically as

$$\dot{\vec{p}} = u \frac{||\vec{p} - \vec{c}_n||}{\hat{t} \cdot (\vec{p} - \vec{c}_n)} \hat{t} \tag{2}$$

where, as before, u represents the controlled growth rate. The scalar term maps growth rate to tip speed and is needed because the tip velocity vector is aligned with the obstacle contour rather than the body's axis. Note that $||\dot{\vec{p}}|| \geq u$ and that when $\hat{t}$ and the robot's body are parallel, the tip speed is equal to the growth rate of the robot and as $\hat{t}$ and the robot's body approach perpendicular orientations, the tip speed grows without bound. Growth along a perpendicular surface is a singularity of the obstacle interaction model and its behavior cannot be predicted in this situation.

III. Path Computation

In this section, we describe a recursive algorithm for integrating the differential obstacle interaction kinematics to determine the path of the tip of the robot while growing through a two-dimensional environment with obstacles.

A. Preliminaries

We assume the following information is provided:

- A discretization of $\mathbb{R}^2$, Z, and a planar map of the environment that contains the discretized location of all obstacles, $M \subset Z$
- An obstacle set, $\mathbf{O}$, which consists of the connected subsets of M. $M = \bigcup_{O \in \mathbf{O}} O$
- Initial state of the robot: $\vec{p}, \vec{c}_1$
- Final length of the robot, L

We will make use of the following notation:

- $\mathrm{O}(\vec{x}) \in \mathbf{O}$ refers to the unique obstacle that contains point $\vec{x}$
- $P_L^{\vec{a},\vec{b}}$ refers to a line of length L that goes through points $\vec{a}$ and $\vec{b}$ and has length L (i.e. $P_L^{\vec{a},\vec{b}} = \left\{ \vec{a} + l \frac{\vec{b}-\vec{a}}{||\vec{b}-\vec{a}||} \mid l \in [0, L] \right\}$)

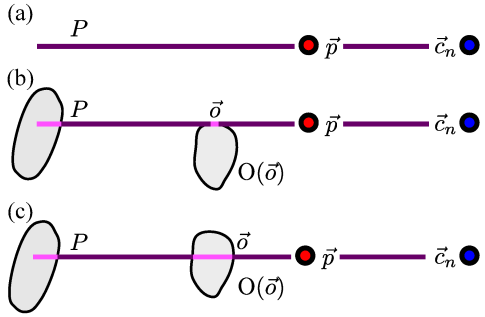

Fig. 5. Three cases in Alg. 1. (a) Free growth not disturbed by an obstacle (corresponds to lines 4 and 5). (b) Most proximal obstacle contact past $\vec{c}_n$ is a glancing contact (corresponds to lines 10 and 11). (c) Most proximal contact past $\vec{c}_n$ is a head-on contact (corresponds to lines 8 and 9).

- NBD($\vec{x}$) refers to the set of neighboring points of $\vec{x}$ that are in $\mathbf{O}(\vec{x})$.
- BOR(O) $\subset O$ refers to the set of points in an obstacle that are on its border (i.e. they have neighboring points that are not in the obstacle).

B. Algorithm Overview

Alg. 1 and Fig. 7 provide a high-level overview of the recursive path computation algorithm. The algorithm takes as input the initial state of the growing robot (Sec. II-A) as well as a desired length that the growing robot will reach. The output of the algorithm is the robot's tip position when it has grown to the final length, L.

The integral curve of free growth differential kinematics is simply the line, $P_{L_r}^{\vec{c}_n,\vec{p}}$, which goes through the robot tip, $\vec{p}$, and most distal contact point, $\vec{c}_n$. L_r is the remaining length to grow (calculated on line 2 of Alg. 1). We let $P_d = P \cap M$ be the obstacle points that disrupt the free growth trajectory of the growing robot. P_d is computed on line 3 of Alg. 1 and it is depicted in Figs. 5(b) and 5(c).

If $P_D = \emptyset$, the robot will grow to its final length without intersecting an obstacle, hence its tip path is simply P and its final tip point is given in line 5 of the algorithm (also depicted in Fig. 5 (a)). Otherwise, $P \cap M \neq \emptyset$ and obstacle interaction must be considered.

Algorithm 1 Recursive Path Computation Algorithm

Input Model state and desired length
Output Tip position at desired length

1: **procedure** PATH($\vec{p}, [\vec{c}_1, \ldots, \vec{c}_n], L$)
2: $L_r \leftarrow L - \sum_{i=1}^{n-1} ||\vec{c}_{i+1} - \vec{c}_i||$
3: $P_d \leftarrow P_{L_r}^{\vec{c}_n,\vec{p}} \bigcap M$
4: **if** $P_d = \emptyset$ **then**
5: **return** $\vec{c}_n + L_r \frac{\vec{p}-\vec{c}_n}{||\vec{p}-\vec{c}_n||}$
6: **end if**
7: $\vec{o} \leftarrow \arg\min_{\vec{x} \in P_d} (\vec{x} - \vec{c}_n) \cdot (\vec{p} - \vec{c}_n)$
8: **if** $P_d \cap \mathrm{O}(\vec{o}) \not\subseteq \mathrm{BOR}(\mathrm{O}(\vec{o}))$ **then**
9: **return** HEADONCP($\vec{p}, [\vec{c}_1, \ldots, \vec{c}_n], \vec{o}, L$)
10: **else**
11: $P_{do} = P_d \bigcap \mathrm{O}(\vec{o})$
12: **return** GLANCINGCP($\vec{p}, [\vec{c}_1, \ldots, \vec{c}_n], P_{do}, L$)
13: **end if**
14: **end procedure**

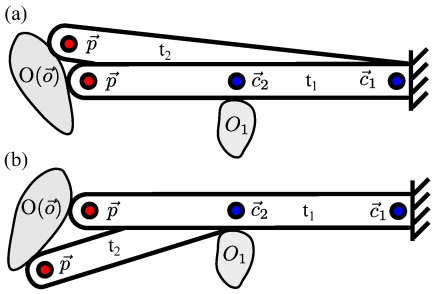

Fig. 6. Two examples of head-on contact paths. In (a), $\vec{c}_2$ is removed from the system state as lateral deflection due to contact with O($\vec{o}$) causes the robot backbone to move away from O_1. This condition is checked on lines 5 and 6 of Alg. 2. In (b), the robot maintains contact with O_1 and pivots about $\vec{c}_2$ while its tip slides along O($\vec{o}$).

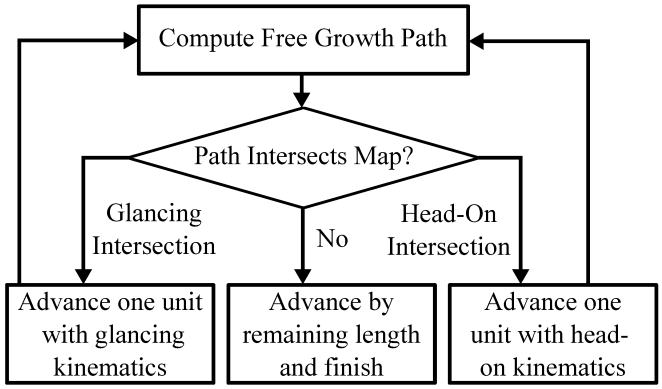

Fig. 7. Flowchart of high-level logic in Alg. 1

C. Integrating Differential Obstacle Interaction Kinematics

At this point in Alg. 1, we assume $P_d \neq \emptyset$, or in other words, the robot tip will collide with an obstacle. We let $\vec{o} \in P_d$ be the most proximal obstacle intersection point (computed on line 7 of Alg. 1) and O($\vec{o}$) be the corresponding obstacle that contains $\vec{o}$. There are two cases that must be handled: a head-on contact between the tip of the robot and O($\vec{o}$), which is handled on lines 8 and 9 of Alg. 1 and a glancing contact of the robot and O($\vec{o}$), which is handled on lines 10 and 11 of Alg. 1. These two cases are described in Sec. III-D and Sec. III-E, respectively.

D. Head-On Contact Path

Head-on contact occurs when the tip of the growing robot is in contact with an obstacle. Two examples of head-on contact are depicted in Figs. 3 and 4. The kinematics of this interaction are described by Eq. 2, which says that the robot tip will simply follow the contour of obstacle $\vec{O}(\vec{o})$.

To integrate Eq. 2, we find the neighboring points of $\vec{o}$ that are on the border of O($\vec{o}$) (line 2 of Alg. 2). Eq. 2 states that $\vec{p}$ will move to one of these points in the direction that is most aligned with the distal segment of the robot's backbone (determined on line 4 of Alg. 2). After sliding the tip along the obstacle one step, the most distal contact point,

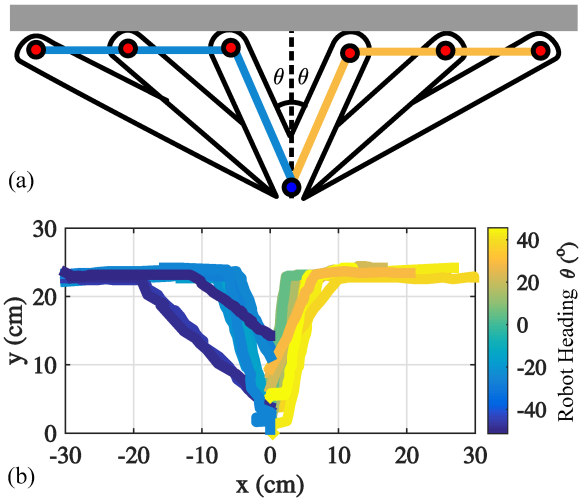

Fig. 8. Experimental trajectories of robot tip position when the robot comes into contact with a wall. (a) Schematic showing two example trajectories and relevant parameters. (b) Experimental trajectories from 20 trials of the robot. As predicted by the model, the tip follows the wall trajectory, to the right if θ is positive, to the left if negative.

$\vec{c}_n$, may have moved out of contact with M as depicted in Fig. 6(a). (Technically, if several obstacles were arranged perfectly tangent to the robot's body, multiple contact points would need to be removed, but we ignore this special-case for the sake of brevity.) Lines 5 and 6 of Alg. 2 check for this condition and if it is satisfied, strip the most distal contact point from the system state. Fig. 6(b) shows a case when the condition is not satisfied and the most distal contact point remains in the system state. Finally, Alg. 1 is recursively called with the updated tip point and updated contact points.

E. Glancing Contact Path

A glancing contact is depicted in Fig. 5(b) and corresponds to the case that the free growth obstructions, P_d, are restricted to the border of $\mathrm{O}(\vec{o})$. A new glancing contact can arise in three situations: (i) The robot is situated so that it will glance an obstacle as its tip grows past the obstacle (a pathological case). (ii) The robot grew past an obstacle it was in head-on contact with. This case is shown in Fig. 3(c). (iii) The robot's backbone comes into contact with a new obstacle as a result of lateral movement (for example, due to interactions with a more distal obstacle).

A glancing contact path is handled by adding a new contact point to the model state that is computed on line 2 of Alg. 3. It corresponds to the most distal point of $\mathrm{O}(\vec{o})$ (Fig. 5(c)). Next we check if the new contact point is more distal than $\vec{p}$. This would be true if a glancing contact arises from cases (i) or (ii) above. If it is, we move $\vec{p}$ slightly past (by ϵ) $\vec{c}_{n+1}$. This is implemented on lines 3 and 4 of Alg. 3. Finally, we recursively call the high level path computation algorithm with the updated model state.

Algorithm 2 Head On Contact Path

Input Model state, proximal intersection point, desired length
Output Tip position at desired length

1: **procedure** HEADONCP($\vec{p}, [\vec{c}_1, \ldots, \vec{c}_n], \vec{o}, L$)
2: $\quad$ BP $\leftarrow$ NBD($\vec{o}$) $\cap$ BOR(O($\vec{o}$))
3: $\quad$ CP $\leftarrow [\vec{c}_1, \ldots, \vec{c}_n]$
4: $\quad$ $\vec{o}_n \leftarrow \arg\max_{\vec{x} \in \mathrm{BP}} (\vec{x} - \vec{o}) \cdot (\vec{p} - \vec{c}_n)$
5: $\quad$ **if** $P^{\vec{c}_n, \vec{o}_n}_{||\vec{o}_n - \vec{c}_n||} \bigcap \mathrm{O}(\vec{o}) = \emptyset$ **then**
6: $\quad\quad$ CP $\leftarrow [\vec{c}_1, \ldots, \vec{c}_{n-1}]$
7: $\quad$ **end if**
8: $\quad$ **return** PATH($\vec{o}_n$, CP, L)
9: **end procedure**

IV. Experimental Results

In this section, we describe experiments that were performed to test both the obstacle interaction model and path computation algorithm presented in Sec. II and Sec. III. We start with experiments that test obstacle interactions with basic shapes such as walls and circles, and end with a more complex scenario that chains multiple obstacle interactions together. For all experiments, a 1.6 cm diameter robot made out of 5 mm thick polyethylene was used. Air pressures between 7 and 28 kPa were used to propel the robot.

A. Growth Into a Wall

As may be seen from Algs. 1 and 2 and depicted in Fig. 3, our model predicts a simple behavior from the robot when it grows into contact with a wall: the tip will slide along the wall's contour, pivoting about the most distal contact point, $\vec{c}_n$. The model predicts that the robot will slide in the direction that is most tangent to the robot's approach path.

To test this model, we performed an experiment in which we repeatedly grew the robot toward a wall from different approach angles. An overhead camera was used to capture the trials. Using color-based image segmentation, we extracted the position of the robot's tip over the course of each trial growth, forming a tip trajectory. Fig. 8(a) illustrates two example starting angles, with the paths the obstacle interaction model predicted and their corresponding tip trajectories in colored lines. Fig. 8(b) shows the results of the experiment, with 20 trial growths. Trajectories were colored by approach angle (0° corresponding to perpendicular to the wall). As predicted, the robot slid along the wall in the direction most tangent to its approach angle.

Algorithm 3 Glancing Contact Path

Input Model state, free growth obstructions, desired length
Output Tip position at desired length

1: **procedure** GLANCINGCP($\vec{p}, [\vec{c}_1, \ldots, \vec{c}_n], P_d, L$)
2: $\quad$ $\vec{c}_{n+1} \leftarrow \arg\max_{\vec{x} \in P_d} (\vec{x} - \vec{c}_n) \cdot (\vec{p} - \vec{c}_n)$
3: $\quad$ **if** $||\vec{p} - \vec{c}_n|| < ||\vec{c}_{n+1} - \vec{c}_n||$ **then**
4: $\quad\quad$ $\vec{p} \leftarrow \vec{c}_{n+1} + \epsilon(\vec{c}_{n+1} - \vec{c}_n)$
5: $\quad$ **end if**
6: $\quad$ **return** PATH($\vec{p}, [\vec{c}_1, \ldots, \vec{c}_{n+1}], L$)
7: **end procedure**

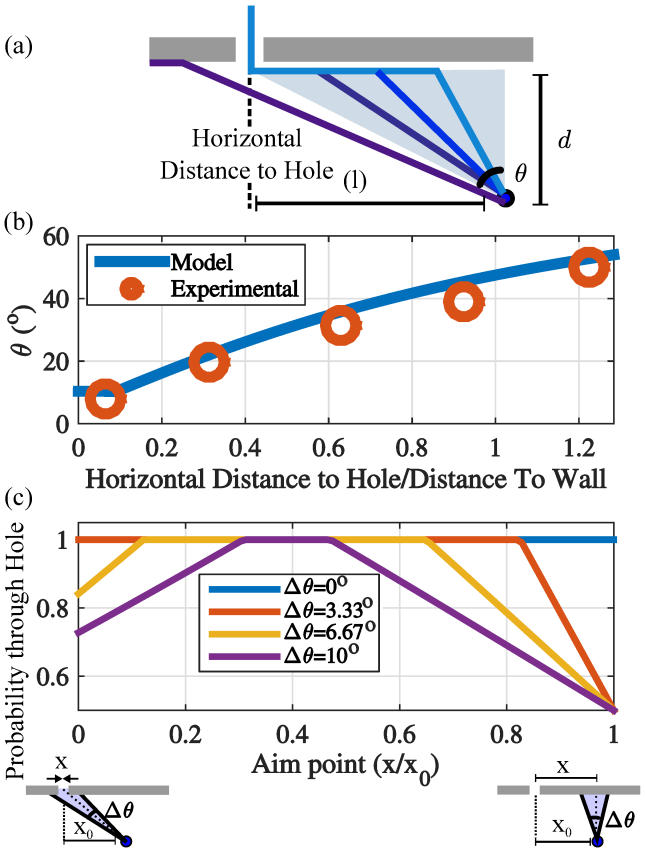

Fig. 9. Experiment of growth through a hole-in-the-wall. (a) Several predicted trajectories of the tip of the growing robot for different approach angles are shown at a fixed distance from the hole. When the approach angle is within the light blue region with solid angle, θ, the robot will grow through the hole. (b) Acceptable solid angle of initial orientations vs horizontal distance from hole. (c) Probability of successfully growing through a hole when there is uniform angular uncertainty ($\Delta\theta$) versus horizontal point the robot is nominally aimed at (x), from a fixed location x_0. This plot indicates that with any uncertainty, it is better to aim to the side of the hole than at it.

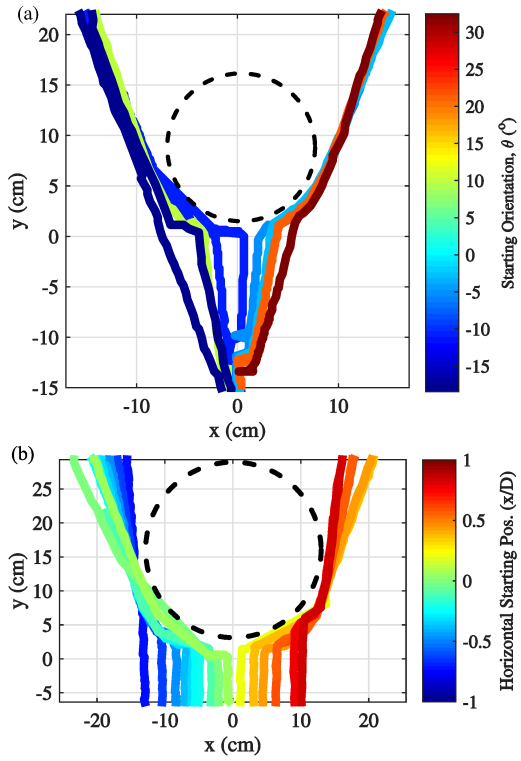

Fig. 10. Experimental trajectories during interaction of the robot with a circular obstacle. (a) Robot was grown from a fixed starting position with varying orientations, shown by color coding. Trajectories after the obstacle are bimodal, with little variability in each mode. (b) Robot was grown with fixed starting orientation and varying position. Trajectories after the obstacle are bimodal, with orientation variability in each mode, but intersect each other; the circular obstacle transforms uncertainty in approach position to variability in orientation.

B. Growth Through a Hole in a Wall

A major feature of the soft growing robot relevant for applications such as search and rescue, inspection, and mining is its ability to penetrate tight spaces [18]. To study this behavior, we performed an experiment in which we repeatedly grew the robot through a hole in the wall, with a width of 6.5 cm (Fig. 9(a)). From Sec. IV-A, we know that if the robot is angled left of vertical, its tip will move along the wall to the left. Furthermore, the model predicts that if the ray extending from $\vec{p}$ in the direction of $\vec{p} - \vec{c}_n$ extends into the hole, it will grow through it. In this way, the obstacle serves to passively guide the robot's tip through the hole. Three predicted tip trajectories are shown in Fig. 9(a).

For a fixed horizontal position, the model predicts that the robot will successfully grow through a hole if its starting orientation is within the shaded region in Fig. 9(a). This region has starting orientations that range from just left of perpendicular to $\tan^{-1}(l/d)$ (aiming at the hole) where l is the horizontal distance from the hole and d is the vertical distance from the wall. Fig. 9(b) shows the solid-angle of

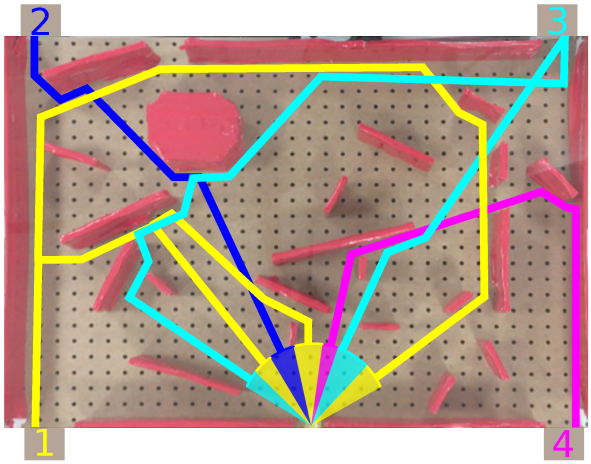

Fig. 11. Obstacle course with tip trajectories computed by Alg. 1. Four exit positions are labeled as 1, 2, 3, and 4 and correspond to colors yellow, blue, cyan, and pink, respectively. Depending on the starting orientation, the robot will end at one of the four locations. Varying over the possible starting orientations, there are seven transitions between ending points. Representative trajectories from each orientation regime is shown, colored to correspond to its ending location.

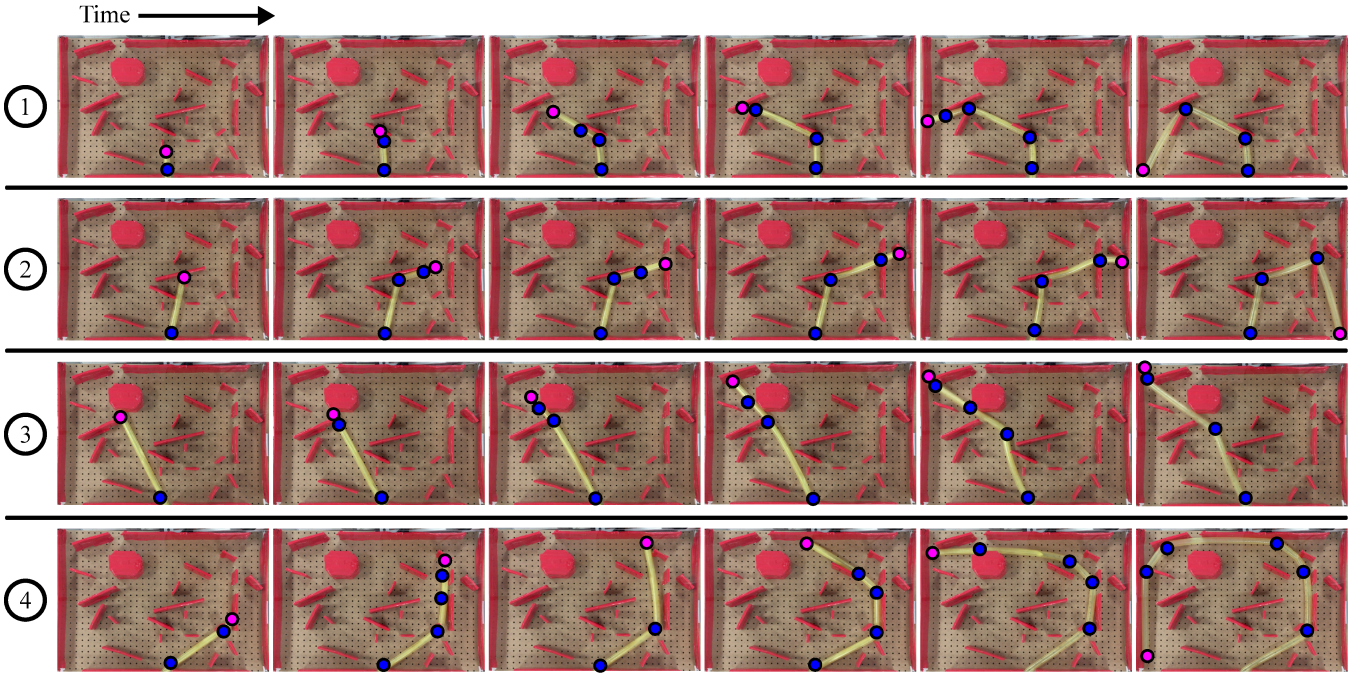

Fig. 12. Stills from key-points (transitions to/from head-on contact and glancing contacts) during four growths of the robot through an obstacle course. All growths start from the same position, but different orientations. Each row corresponds to a growth. Obstacle contact points are denoted by blue circles, and tip positions by pink circles.

starting orientations that will result in successfully growing through the wall-hole versus normalized horizontal distance from the wall for both the model and experimental trials. Fig. 9(c) suggests that in the case that there is uncertainty in the angle of approach, it is better to aim the robot at the wall ($x/x_0 > 0$) rather than aiming directly at the hole ($x/x_0 = 0$).

C. Growth Into a Circular Object

From the perspective of Eq. 2, a circle is a more complicated interaction than a wall, due to its spatially varying contour tangent, therefore we performed two experiments to test interaction of our soft growing robot with a circular obstacle. The first tested growth into a circular obstacle from a fixed position but varying orientation (Fig 4(a)). Starting orientations varied from $-19°$ to $19°$, with $0°$ corresponding to vertical. The second tested growth into a circular obstacle from a varying position, but fixed orientation (Fig. 4(b)). Starting horizontal positions ranged from -15 cm to 15 cm, with 0 cm corresponding to the center of the object.

Both experiments involved repeated trials that were captured with an overhead camera. As before, the tip trajectory was computed from the video recordings. For the first experiment (fixed position, varied orientation), the model predicts that all starting orientations will end up in one of two trajectory modes, with zero variability in each mode, depending on whether the starting orientation was to the left or the right of vertical. The experimental data supports this prediction with a standard deviation of final trajectory orientations of $\approx 3°$ in each mode. Measured orientation variability is likely due to measurement precision. For the second experiment (fixed orientation, varied position), the model predicts that the trajectories after the obstacle will be bimodal with orientation variability, but little position variability. Again, the data supports this with a standard deviation of final trajectory orientations of $\approx 16°$.

D. Growth Through a Cluttered Environment

To demonstrate the path computation algorithm (Sec. III), we created a planar environment with obstacles to grow the robot through. Fig. 11 shows the obstacle course that was used. It has four possible exits that are labeled 1, 2, 3, and 4. By starting at the same position, but varying the orientation of the growing robot, its path is changed. Sweeping the starting orientation over the range of possible angles, the ending location changes six times. For example, moving the starting orientation from vertical to just right of vertical changes the ending location from the lower-left corner (1) to the lower-right corner (4). Representative tip trajectories predicted by Alg. 1 are overlaid in Fig. 11. The path computation algorithm correctly predicted all exit locations. Fig. 12 shows stills from four growths of the robot through the cluttered environment, one to each of the four corners. A deviation from the model is shown in trial 4 when the robot is pushed away from an obstacle due to more distal interactions of the robot's tip. The path of the robot's tip is still correctly predicted in spite of this deviation because of the shape of the map.

V. Conclusion and Future Work

For robots moving through cluttered environments, it is inevitable that the robot will interact with obstacles. Rather than being inherently negative, obstacle interactions can be advantageous for navigating the growing robot to a particular

destination, since interactions with obstacles can consolidate many possible paths down to a single desired path and these interactions can direct the robot to locations not on a straight line path from its starting point. Though this principle was shown for the specific case of a soft growing robot, it applies more broadly to any robot that passively follows the contour of an obstacle.

Our path computation method has several limitations. An assumption of head-on contact (Secs. II and III-D) is that the robot's backbone will pivot about the most distal contact point as its tip slides along an obstacle contour. This is only true when the robot (i) buckles and (ii) the cause of buckling is a transverse rather than axial load. These assumptions are satisfied when the membrane material is sufficiently thin, air pressure in the backbone is low enough, the free length is short enough, and the angle of contact is above a few degrees (Sec. II-B.2). If these are not true, the robot will either bend, or buckle at a point that is more distal than the last contact point. Though it will not affect the accuracy of the predicted tip location for a single obstacle, it could affect the direction of the most distal segment of the robot ($\vec{c}_n$ to $\vec{p}$), and thus the accuracy of tip predictions for multiple, chained obstacle interactions (using, for example, Alg. 1). In addition, we do not consider interactions with compliant obstacles. Future work will investigate the effect of obstacle compliance on the accuracy of the model.

The obstacle interaction model presented and experimentally verified in this work can be used to understand and predict the path of a soft growing robot that is growing while interacting with obstacles, an important step for deploying these robots in cluttered environments. Future work will incorporate active steering as described in [18] into the obstacle interaction model. Depending on the layout of obstacles, not all locations can be reached with open-loop control, making some active steering critical for full exploration. Thus, we plan to integrate the proposed algorithm into a planner to find paths to a destination that reduce the need for active steering by moving toward obstacles when beneficial, potentially minimizing the complexity of robot design as well as the probability that an erroneous steering event occurs. Further, since obstacles can reduce uncertainty, such a minimally actuated control scheme could allow soft robots to more accurately navigate to target locations.

ACKNOWLEDGMENTS

The authors thank Dan Goldman for his contributions to concept development.

REFERENCES

[1] O. Khatib, "Real-time obstacle avoidance for manipulators and mobile robots," *The International Journal of Robotics Research*, vol. 5, no. 1, pp. 90–98, 1986.

[2] S. M. LaValle, *Planning Algorithms*. Cambridge University Press, 2006.

[3] R. M. Murray and S. S. Sastry, "Nonholonomic motion planning: Steering using sinusoids," *IEEE Transactions on Automatic Control*, vol. 38, no. 5, pp. 700–716, 1993.

[4] J. P. Desai, J. P. Ostrowski, and V. Kumar, "Modeling and control of formations of nonholonomic mobile robots," *IEEE Transactions on Robotics and Automation*, vol. 17, no. 6, pp. 905–908, 2001.

[5] Y. S. Nam, B. H. Lee, and M. S. Kim, "View-time based moving obstacle avoidance using stochastic prediction of obstacle motion," in *IEEE International Conference on Robotics and Automation*, 1996, pp. 1081–1086.

[6] D. Rus and M. T. Tolley, "Design, fabrication and control of soft robots," *Nature*, vol. 521, no. 7553, pp. 467–475, 2015.

[7] Y.-F. Zheng and H. Hemami, "Mathematical modeling of a robot collision with its environment," *Journal of Field Robotics*, vol. 2, no. 3, pp. 289–307, 1985.

[8] M. K. Vukobratović and V. Potkonjak, "Dynamics of contact tasks in robotics. Part I: general model of robot interacting with environment," *Mechanism and machine theory*, vol. 34, no. 6, pp. 923–942, 1999.

[9] A. Petrovskaya, J. Park, and O. Khatib, "Probabilistic estimation of whole body contacts for multi-contact robot control," in *IEEE International Conference on Robotics and Automation*, 2007, pp. 568–573.

[10] E. Coevoet, A. Escande, and C. Duriez, "Optimization-based inverse model of soft robots with contact handling," *IEEE Robotics and Automation Letters*, vol. 2, no. 3, pp. 1413–1419, 2017.

[11] M. C. Yip and D. B. Camarillo, "Model-less feedback control of continuum manipulators in constrained environments," *IEEE Transactions on Robotics*, vol. 30, no. 4, pp. 880–889, 2014.

[12] M. J. Travers, J. Whitman, P. Schiebel, D. I. Goldman, and H. Choset, "Shape-based compliance in locomotion." in *Robotics: Science and Systems*, 2016.

[13] F. Qian and D. I. Goldman, "The dynamics of legged locomotion in heterogeneous terrain: universality in scattering and sensitivity to initial conditions." in *Robotics: Science and Systems*, 2015.

[14] A. A. Transeth, R. I. Leine, C. Glocker, K. Y. Pettersen, and P. Liljebäck, "Snake robot obstacle-aided locomotion: Modeling, simulations, and experiments," *IEEE Transactions on Robotics*, vol. 24, no. 1, pp. 88–104, 2008.

[15] P. Liljeback, K. Y. Pettersen, and O. Stavdahl, "Modelling and control of obstacle-aided snake robot locomotion based on jam resolution," in *IEEE International Conference on Robotics and Automation*, 2009, pp. 3807–3814.

[16] P. Liljeback, K. Y. Pettersen, Ø. Stavdahl, and J. T. Gravdahl, "Snake robot locomotion in environments with obstacles," *IEEE/ASME Transactions on Mechatronics*, vol. 17, no. 6, pp. 1158–1169, 2012.

[17] S.-g. Roh and H. R. Choi, "Differential-drive in-pipe robot for moving inside urban gas pipelines," *IEEE transactions on robotics*, vol. 21, no. 1, pp. 1–17, 2005.

[18] E. W. Hawkes, L. H. Blumenschein, J. D. Greer, and A. M. Okamura, "A soft robot that navigates its environment through growth," *Science Robotics*, vol. 2, no. 8, p. eaan3028, 2017.

[19] J. D. Greer, T. K. Morimoto, A. M. Okamura, and E. W. Hawkes, "Series pneumatic artificial muscles (sPAMs) and application to a soft continuum robot," in *IEEE International Conference on Robotics and Automation*, 2017, pp. 5503–5510.

[20] L. H. Blumenschein, L. Gan, J. Fan, A. M. Okamura, and E. W. Hawkes, "A tip-extending soft robot enables reconfigurable and deployable antennas," *IEEE Robotics and Automation Letters*, vol. 3, no. 2, pp. 949–956, 2018.

[21] L. H. Blumenschein, N. S. Usevitch, B. Do, E. W. Hawkes, and A. M. Okamura, "Helical actuation on a soft inflated robot body," in *IEEE International Conference on Soft Robotics (RoboSoft), in press*, 2018.

[22] D. Caleb Rucker and R. J. Webster, "Mechanics of continuum robots with external loading and general tendon routing," *Springer Tracts in Advanced Robotics*, vol. 79, no. 6, pp. 645–654, 2014.

[23] W. Park, J. S. Kim, Y. Zhou, N. J. Cowan, A. M. Okamura, and G. S. Chirikjian, "Diffusion-based motion planning for a nonholonomic flexible needle model," in *IEEE International Conference on Robotics and Automation*, 2005, pp. 4600–4605.

[24] R. J. Webster and B. A. Jones, "Design and Kinematic Modeling of Constant Curvature Continuum Robots: A Review," *The International Journal of Robotics Research*, vol. 29, no. 13, pp. 1661–1683, 2010.

[25] P. Masser, R. Page, and W. Stoner, "Deflections of an inflated circular-cylindrical cantilever beam," *AIAA journal*, vol. 1, no. 7, 1963.

[26] W. Fichter, "A theory for inflated thin-wall cylindrical beams," 1966.

[27] Z. M. Hammond, N. S. Usevitch, E. W. Hawkes, and S. Follmer, "Pneumatic reel actuator: Design, modeling, and implementation," in *IEEE International Conference on Robotics and Automation*. IEEE, 2017, pp. 626–633.